

## Supporting Information

# A Bi/BiOCl Heterojunction Photocatalyst with Enhanced Electron-Hole Separation and Excellent Visible Light Photodegrading Activity

Yu Yu,<sup>a</sup> Changyan Cao,<sup>a</sup> Hua Liu,<sup>a</sup> Ping Li,<sup>a</sup> Fangfang Wei,<sup>b</sup> Yan Jiang,<sup>b</sup> Weiguo Song<sup>\*[a](#)</sup>

<sup>a</sup> Laboratory of Molecular Nanostructures and Nanotechnology, Institute of Chemistry, Chinese Academy of Sciences & Beijing National Laboratory of Molecular Sciences. Beijing, 100190, P. R. China

<sup>b</sup> Graduate University of Chinese Academy of Sciences, Beijing, 100049, P. R. China

\* E-mail: wsong@iccas.ac.cn

## Experimental Section

**Materials:** Bismuth nitrate hydrate ( $\text{Bi}(\text{NO}_3)_3 \cdot 5\text{H}_2\text{O}$ ), Cetyltrimethyl ammonium bromide (CTAB), Hydrochloric acid (HCl, 36.7%), Ascorbic acid (AC), Isopropyl alcohol (IPA), Triethanolamine (TEOA), Nitroblue tetrazolium (NBT), Acetophenone (AP) and ethanol were from Sinopharm Chemical Reagent Co., Ltd. 4-Chlorobenzaldehyde (CBD) was purchased from Alfa. Rhodamine B (RhB), Methylblue (MB), Coomassie brilliant blue (CBB) and Eosin B were purchased from Aladdin. All the reagents were analytically pure and used without further purification. Commercial BiOCl and Bi metal powders were purchased from Sigma-Aldrich. P25  $\text{TiO}_2$  was from Degussa Corp.

**Synthesis of Bi/BiOCl heterojunction:** 3 mmol of  $\text{Bi}(\text{NO}_3)_3 \cdot 5\text{H}_2\text{O}$  were added into 5 ml EtOH dissolving 0.3 g CTAB. After white slurry was formed, 0.5 ml HCl were dropwise added and mixed uniformly by stirring for a while. These mixtures were transferred into a 40 ml Teflon-lined stainless steel autoclave to perform hydrothermal process at 180 °C for 5 h. After completion of the hydrothermal reaction, the product was washed using absolute ethanol and deionized water several times to remove the surfactant, then dried at 80 °C at air atmosphere.

**Characterization:** X-ray diffraction (XRD) patterns were recorded on a Rigaku diffractometer (Maxima XRD-7000) using Cu Ka irradiation. SEM image was taken on scanning electron microscopy (JEOL-6701F). TEM images and EDS results were taken on transmission electron microscopy (Tecnai G2 F20 U-TWIN). The UV-visible absorption spectra of catalysts were obtained by using a UV-visible spectrophotometer (UV-2550, Shimadzu, Japan).  $\text{BaSO}_4$  was used as a reflectance standard. Electron paramagnetic resonance (EPR) measurements were performed with a Bruker ESP-300 ESR

spectrometer at room temperature. The settings for the ESR spectrometer were: center field 3488 G; modulation frequency 100 kHz; microwave frequency 9.75 GHz; power 12.9 mW. XPS and Raman scattering investigations were carried on the ESCALab220i-XL photoelectron spectroscopy and Thermo Scientific DXR Raman microscope using a 532 nm laser, respectively. Photoluminescence (PL) spectra were characterized using a Hitachi F-4500 spectrophotometer with  $\lambda_{\text{exc}} = 320$  nm.

**Photodegradation performance measurements:** The photocatalytic activity of the samples was evaluated in terms of the photodegradation of dyes and persistent organic pollutants (POP) under visible light irradiation at ambient temperature. 50 mg of catalyst was added into a 100 mL of 10 mg/L dye aqueous solution to undergo a stirring in the dark for 1 h. After reaching a complete adsorption–desorption equilibrium, it was exposed to visible light irradiation offered by 50 W Xe lamp with a 420 nm cut-off filter under continuous stirring. The vertical distance between lamp and liquid level is 20 cm. A small quantity of liquid was sampled at the interval of 1 min to measure variation of the concentration of dye in the solution. The concentrations of RhB, MB, CBB and Eosin B were determined from the absorbance at the wavelength of 554, 598, 618, and 528 nm respectively by an UV-visible spectrophotometer (UV-2550, Shimadzu, Japan). The same procedure was also done for P25, dodecahedron  $\text{Ag}_3\text{PO}_4$ , and commercial BiOCl for comparison. Catalysts were centrifuged out and washed for the recyclable catalysis. The photodegradation was also carried under different atmosphere by bubbling  $\text{N}_2$  or  $\text{O}_2$  into the solution during both the adsorption process in dark and photodegradation experiments under irradiation. The photodegradations of acetophenone and 4-chlorobenzaldehyde were operated in 100 mL of 150 mg/L aqueous solution with 100 mg catalyst. The interval time of taking samples was 30 min, and the concentrations of POP were also determinated by UV-visible spectrophotometer.

**Active species trapping and superoxide radical quantification experiments:** The experiments for detecting the active species were similar to photodegradation activity test, except 1.5 mM IPA, AC, and TEOA were added to quench hydroxyl radicals ( $\bullet\text{OH}$ ), superoxide radical ( $\text{O}_2^{\bullet-}$ ) and holes ( $\text{h}^+$ ), respectively. The RhB photodegradation activity test was replaced by NBT ( $5 \times 10^{-5}$  mol/L, absorption peak at 259 nm) to quantify the amount of  $\text{O}_2^{\bullet-}$  generating from Bi/BiOCl photocatalytic system, by quantitatively analyzing the concentration of NBT with Shimadzu UV-2550.

**Controlling Experiments:** The procedures of controlling experiments were similar that of synthesis of Bi/BiOCl heterojunction, while the details of difference in the utilization of regents were list in Table S2 and S3. The phase information and elemental composition of different products by controlling experiments were also displayed in Table S2 and S3.

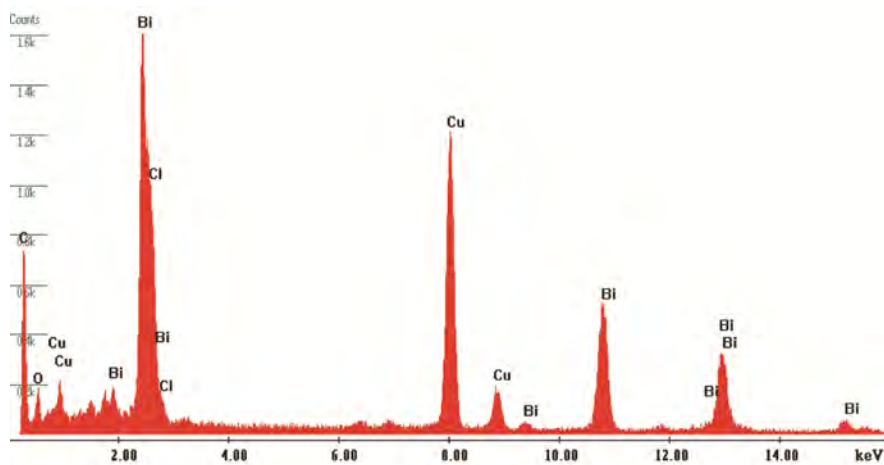


**Figure S1.** EDS results of Bi/BiOCl heterojunction photocatalyst.

**Table S1.** Elemental composition of Bi/BiOCl heterojunction catalyst (At. %) by EDS, XPS and ICP.

Element	Bi	Cl	O	Br	Method
	49.8	31.2	17.6	1.3	EDS
	75.7	13.4	9.2	1.7	XPS
	45.3	31.6	23.1	-	ICP

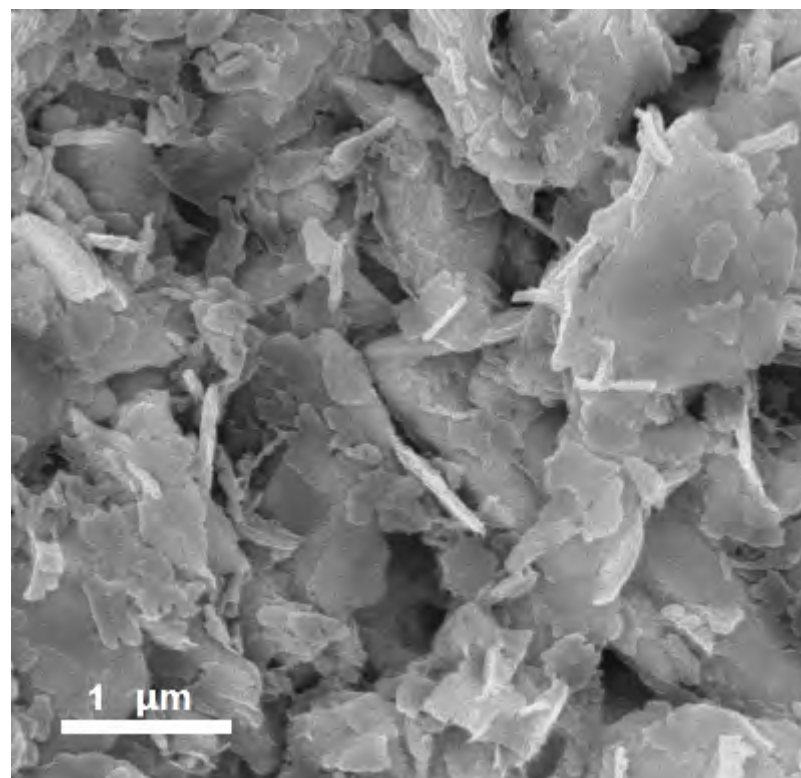


**Figure S2.** The typical SEM image of Bi/BiOCl heterojunction catalyst.

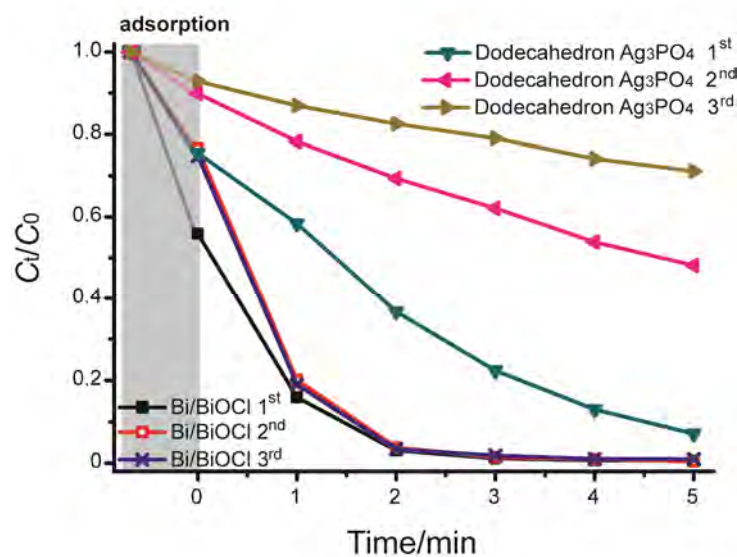


**Figure S3.** The variation of RhB concentration by photocatalytic reaction with Bi/BiOCl and dodecahedron  $\text{Ag}_3\text{PO}_4$ , showing decaying activity of  $\text{Ag}_3\text{PO}_4$  and stable performance of BiOCl in 3 cycles.

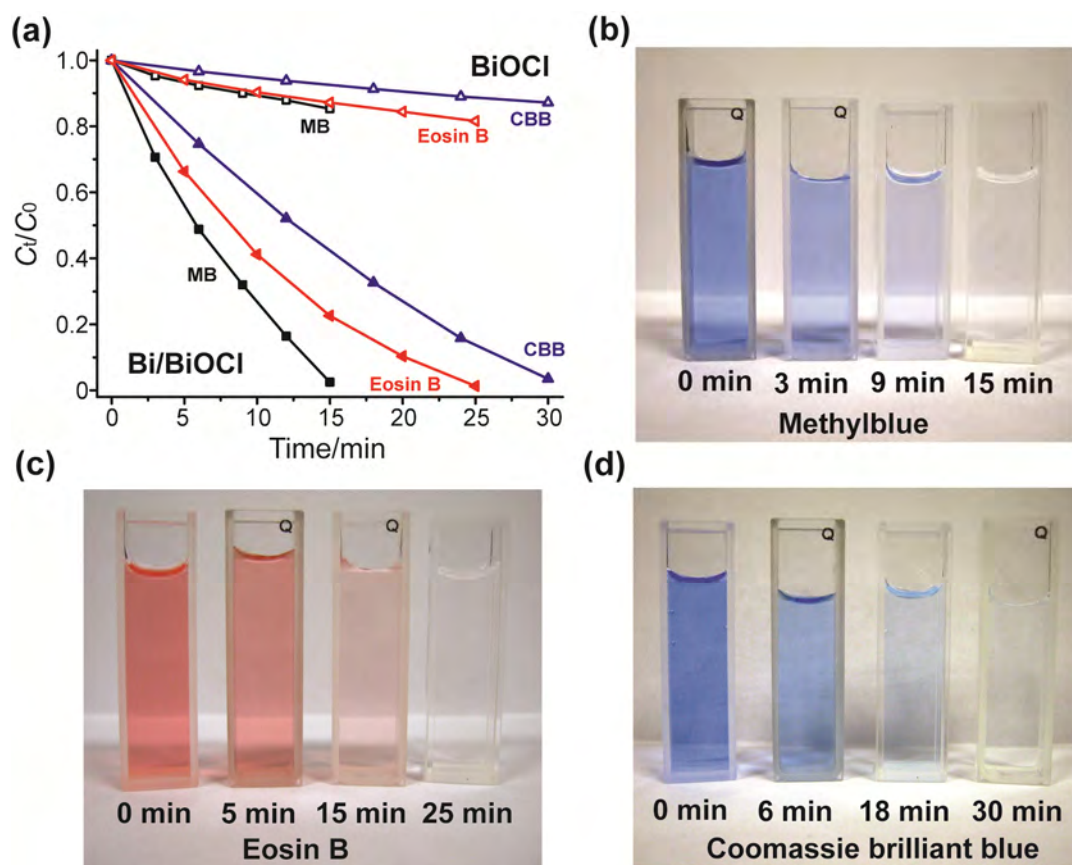


**Figure S4.** (a) Degradation performances for Methylblue (MB), Eosin B, and Coomassie brilliant blue (CCB) over Bi/BiOCl. Photograph image of temporal evolution of MB, Eosin B, and CCB solution over Bi/BiOCl under visible irradiation.

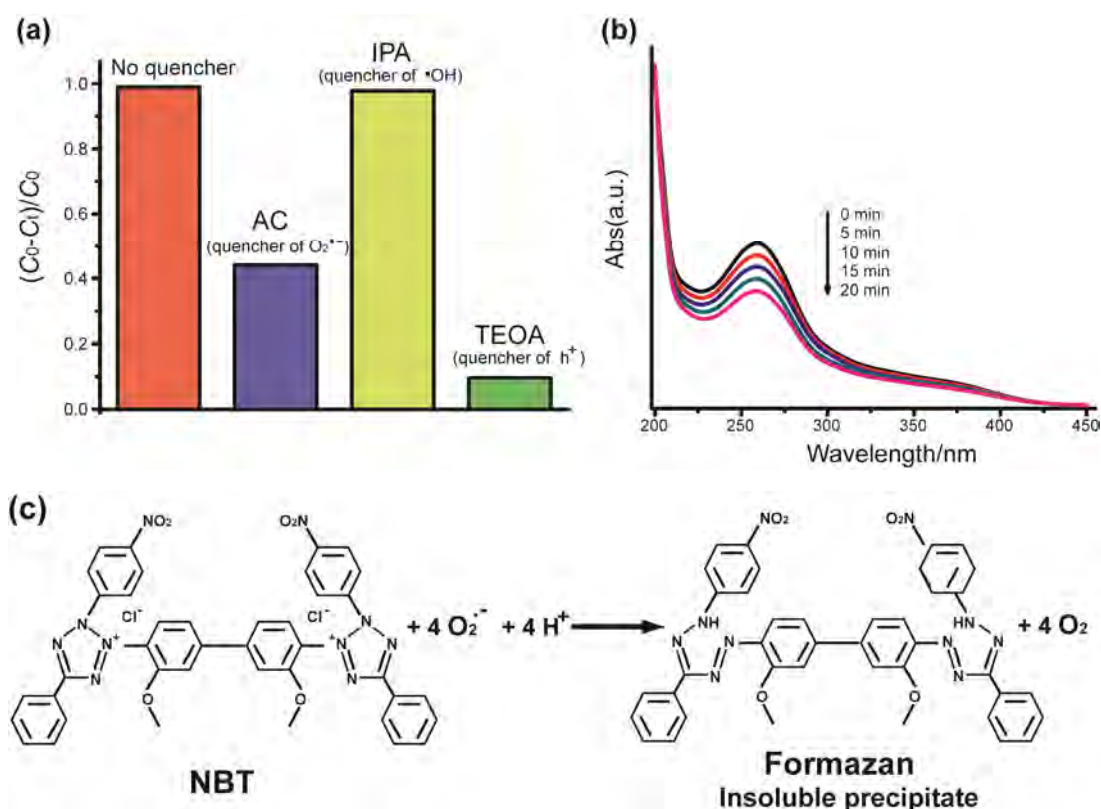


**Figure S5.** (a) The degradation efficiencies ( $C_0 - C_t$ )/ $C_0$  of Bi/BiOCl catalysts for RhB degradation at 5 min with different quenchers (ascorbic acid to  $O_2^{•-}$ , isopropyl alcohol to  $\cdot OH$ , and triethanolamine to  $h^+$ ). (b) The variation of UV-visible absorption spectra of nitroblue tetrazolium under visible light irradiation with the presence of Bi/BiOCl. (c) Reaction of NBT with superoxide ion.

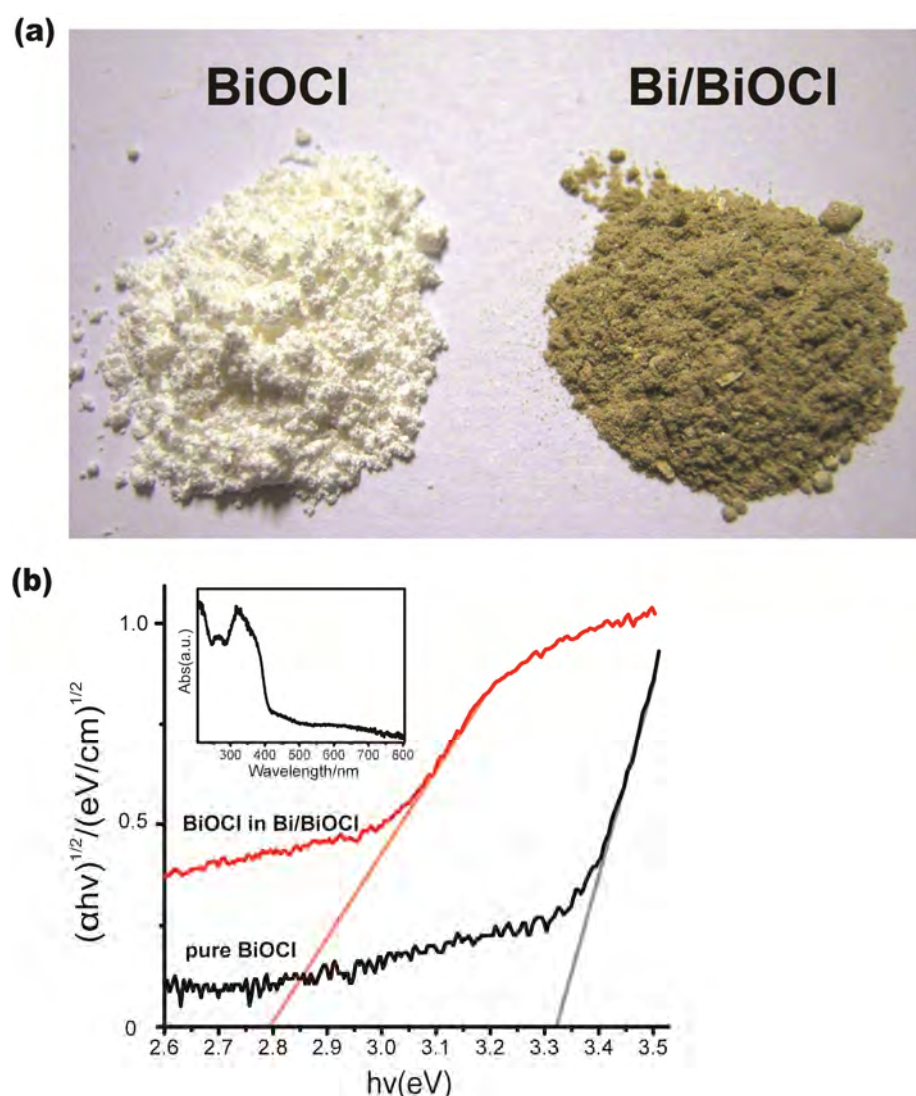


**Figure S6.** (a) Photograph image of BiOCl and Bi/BiOCl. (b) The  $(\alpha h v)^{1/2}$  versus  $h v$  plots of BiOCl in Bi/BiOCl and pure BiOCl. Inset shows the calculated UV-visible absorption spectra of BiOCl in Bi/BiOCl.

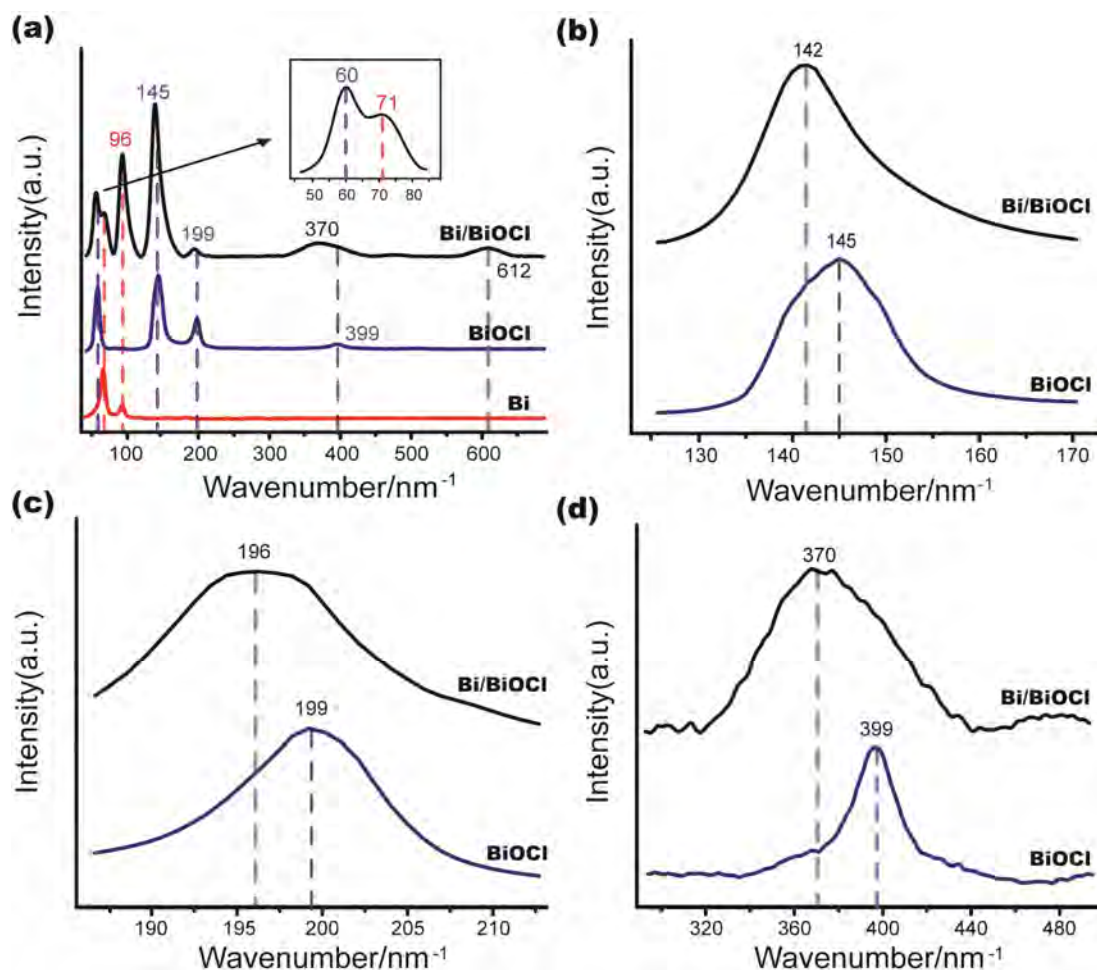


**Figure S7.** (a) Raman spectra of Bi/BiOCl, BiOCl, and Bi. The An expanded view of (b)  $A_{1g}$  internal, (c)  $E_g$  internal Bi-Cl stretching mode bands and (d)  $E_g$  and  $B_{1g}$  oxygen atoms motion band showing red-shift in the peak position.

In Raman spectra of Bi/BiOCl (Figure 4a), both the characteristic peaks of Bi and BiOCl could be observed, which was consistent with the coexistence of Bi and BiOCl depicted by XRD. The  $A_{1g}$  and  $E_g$  internal Bi-Cl stretching bands of BiOCl in Bi/BiOCl shifted to low frequency compared to pure BiOCl ( $145$  and  $199\text{ cm}^{-1}$ ). The red shift was likely due to the low charged and coordinated Bi atom produced by oxygen vacancies (Figure S7).<sup>1,2</sup> A similar red-shift was severe for the weak  $E_g$  and  $B_{1g}$  band involving the motion of the oxygen atoms of BiOCl in Bi/BiOCl (from  $399$  to  $370\text{ cm}^{-1}$ ). The displacement of oxygen atoms due to oxygen vacancies, resulting in the lattice distortion and compressive stress state, was responsible for not only the red-shift but also the intensive broadening of the band.<sup>3-5</sup> A new broad band appeared with a maximum near  $612\text{ cm}^{-1}$  probably resulting from a disorder-induced mixing of the Raman mode with upper optical phonon states. Similar phenomenon had been reported in other materials.<sup>6-8</sup>

**Supplementary Table S2.** Details of controlling experiments-I, elemental composition (At. %, by EDS) and phase information of different products.

	<i>Bi(NO<sub>3</sub>)<sub>3</sub></i>	<i>CTAB</i>	<i>HCl</i>	<i>EtOH</i>	
<i>Sample-1</i>	3 mmol	0.3 g	0.5 mL	0 (6mL H <sub>2</sub> O replacing)	
<i>Sample-2</i>	3 mmol	0.3 g	0	6 mL	
<i>Sample-3</i>	3 mmol	0	0.5 mL	6 mL	
<i>Elemental</i>	<i>Bi</i>	<i>Cl</i>	<i>O</i>	<i>Br</i>	<i>Crystalline Phase</i>
<i>Sample-1</i>	38.7	34.8	25.5	1.0	BiOCl
<i>Sample-2</i>	39	0	24.3	36.7	BiOBr
<i>Sample-3</i>	33.2	30.7	35.9	0.2	BiOCl + Bi <sub>2</sub> O <sub>3</sub> (few)

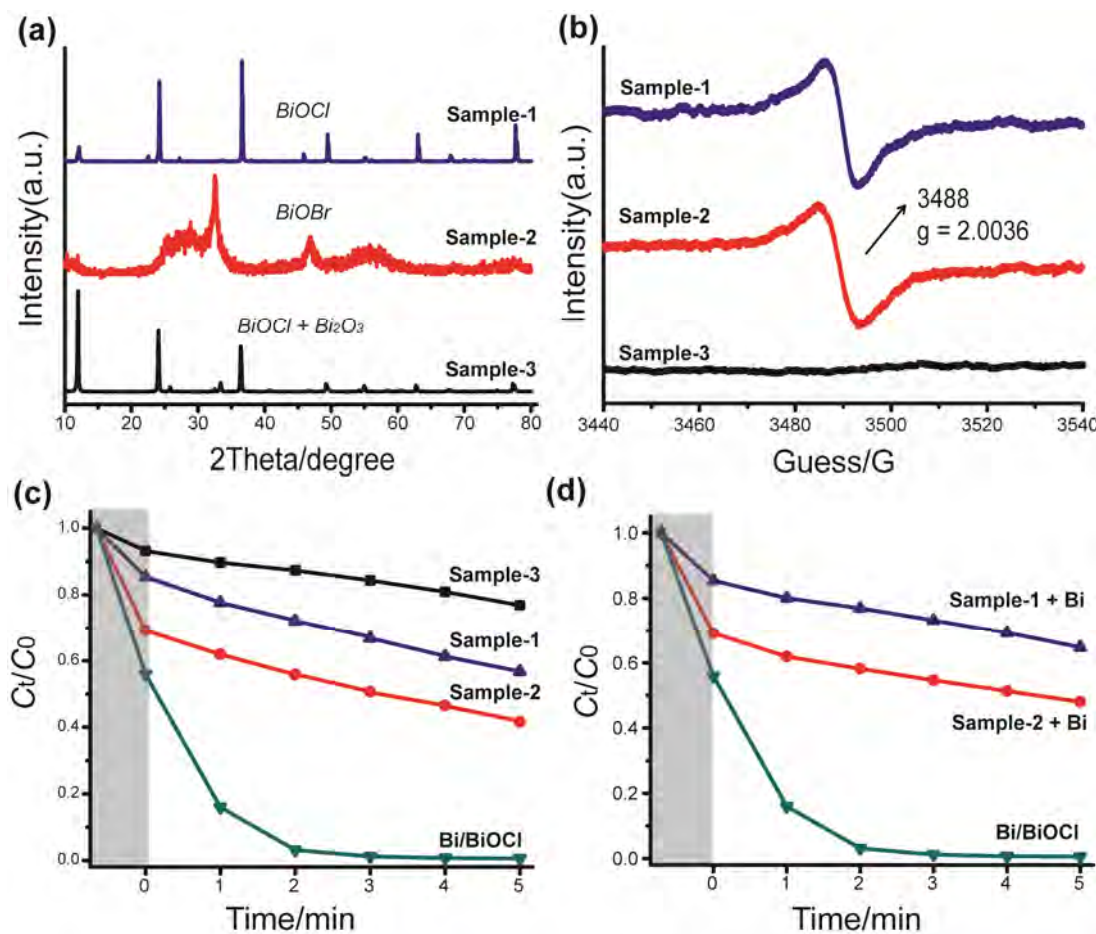


**Figure S8.** XRD pattern (a), EPR spectra (b), and photodegradation performances for RhB of Sample-1 (in H<sub>2</sub>O), Sample-2 (without HCl), and Sample-3 (without CTAB) produced in controlling experiments. (d) photo-degradation performances for RhB of Sample-1 and Sample-2 physically mixed with Bi powder.

BiOCl and few Bi<sub>2</sub>O<sub>3</sub> without oxygen vacancies (Sample1 in Figure S8a, b) were fabricated in the absence of CTAB, we can conclude that the CTAB played a significant role in producing oxygen vacancies in BiOCl. In a typical formation process of BiOCl, Bi<sup>3+</sup> reacted with H<sub>2</sub>O to form hydroxylated compound, and then dehydrations took place between neighboring hydroxyl

groups to form the bismuth oxide-based fluorite-like layers [M<sub>2</sub>O<sub>2</sub>], followed by intergrowth with double chlorine layers to construct such [Cl–Bi–O–Bi–Cl] sheets stack.<sup>9</sup> In the presence of CTAB, the hyamine cation and Cl<sup>-</sup> can produce the complex of C<sub>16</sub>H<sub>33</sub>(CH<sub>3</sub>)<sub>3</sub>N–Cl–Bi with Bi<sup>3+</sup>, which reduced the degree of hydroxylation.<sup>10</sup> During the growth of M<sub>2</sub>O<sub>2</sub> layers, the C<sub>16</sub>H<sub>33</sub>(CH<sub>3</sub>)<sub>3</sub>N–group shed off, leaving oxygen vacancies in BiOCl. In the synthesis of Bi/BiOCl heterojunction, the addition of a large quantity of EtOH and HCl could greatly reduce the rate of generation of BiOCl, considering that was a water-consuming and proton-producing reaction. There was consequently a competition for Bi<sup>3+</sup> between the reaction to BiOCl and reduction to zerovalent Bi. Especially for the EtOH, it not only reacted with Bi<sup>3+</sup> to form alcoholate, the dealcoholization rate of which was extremely less than dehydration of hydroxide, but also enhanced the tendency of “Bi<sup>3+</sup> to Bi<sup>0</sup>” caused by the associative reducibility of alcohol and CTAB.<sup>11</sup> For the reaction Bi<sup>3+</sup> + 3e<sup>-</sup> → Bi(s) (a), E<sub>0'</sub> = 0.32 V, and ethanol oxidation (Ethanol → Acetaldehyde + 2 H<sup>+</sup> + 2 e<sup>-</sup> (b)) has a more negative the redox potential of 0.197 V. There were also some reports about the polyol process in which Bi metal and its alloy was produced by the reducibility of ethylene glycol at a not too high temperature.<sup>12,13</sup> It's reasonable that in our synthesis, the Bi<sup>3+</sup> could be reduced to zerovalent nanoparticles growing on the BiOCl sheets as the equation (a) and (b). As a result, a heterojunction structure consisting of BiOCl sheets with oxygen vacancies and zerovalent Bi nanoparticles was fabricated.

**Supplementary Table S3.** Details of controlling experiments-II, elemental composition (At. %, by ICP) and phase information of different products.

	<i>Bi(NO<sub>3</sub>)<sub>3</sub></i>	<i>CTAB</i>	<i>HCl</i>	<i>EtOH</i>	
<i>Sample-4</i>	3 mmol	0.1 g	0.5 mL	6mL	
<i>Sample-5</i>	3 mmol	0.5 g	0.5 mL	6 mL	
<i>Elemental</i>	<i>Bi</i>	<i>Cl</i>	<i>O</i>	<i>Br</i>	<i>Crystalline Phase</i>
<i>Sample-4</i>	39.3	33.6	27.1	-	BiOCl + Bi
<i>Sample-5</i>	69.7	18.9	11.4	-	Bi + BiOCl

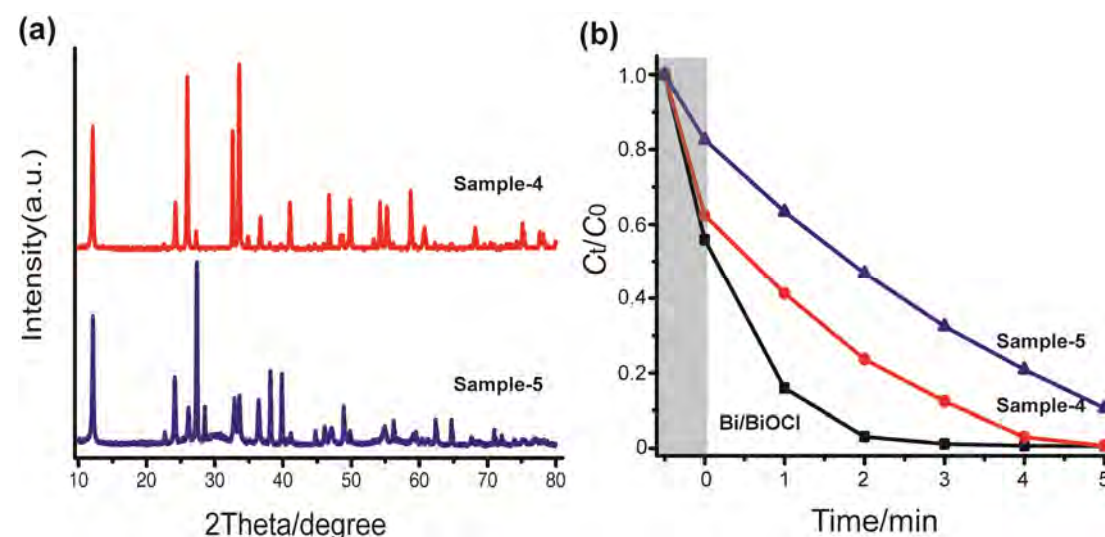


**Figure S9.** XRD pattern (a), and photodegradation performances (b) for RhB of Sample-4 (BiOCl/0.17 Bi) and Sample-5 (BiOCl/ 2.69 Bi).

## References

1. H.-Y. Lu, S.-Y. Chu and S.-H. Cheng, *J. Cryst. Growth*, 2005, **274**, 506-511.
2. J. E. Spanier, R. D. Robinson, F. Zhang, S.-W. Chan and I. P. Herman, *Phys. Rev. B*, 2001, **64**, 245407.
3. Y. Tian, C. F. Guo, Y. Guo, Q. Wang and Q. Liu, *Appl. Surf. Sci.*, 2012, **258**, 1949-1954.
4. Z.-Y. Pu, J.-Q. Lu, M.-F. Luo and Y.-L. Xie, *J. Phys. Chem. C*, 2007, **111**, 18695-18702.
5. Y. Hu, H. Gu, X. Sun, J. You and J. Wang, *Appl. Phys. Lett.*, 2006, **88**, 193120-193123.
6. J. R. McBride, K. C. Hass, B. D. Poindexter and W. H. Weber, *J. Appl. Phys.*, 1994, **76**, 2435-2441.
7. G. A. Kourouklis, A. Jayaraman, B. Batlogg, R. J. Cava, M. Stavola, D. M. Krol, E. A. Rietman and L. F. Schneemeyer, *Phys. Rev. B*, 1987, **36**, 8320-8324.
8. Z. Iqbal, S. W. Steinhauser, A. Bose, N. Cipollini and H. Eckhardt, *Phys. Rev. B*, 1987, **36**, 2283-2286.
9. V. A. K. Dolgikh, L. N. , Russ. *J. Inorg. Chem.*, 1992, **37**, 488.
10. M. Shang, W. Wang and L. Zhang, *J. Hazard. Mater.*, 2009, **167**, 803-809.
11. A. A. Athawale, P. P. Katre, M. Kumar and M. B. Majumdar, *Mater. Chem. Phys.*, 2005, **91**, 507-512.
12. C. Roychowdhury, F. Matsumoto, P. F. Mutolo, H. D. Abruña and F. J. DiSalvo, *Chem. Mater.*, 2005, **17**, 5871-5876.
13. M. F. Figlarz, F.; Lagier, J.-P., *French Patent*, 1985, No. **8221483**.